

## Metallic Magnetic Calorimeters for X-ray Spectroscopy

L. Fleischmann<sup>1</sup>, M. Linck<sup>1</sup>, A. Burck<sup>1</sup>, C. Domesle<sup>1</sup>, C. Höhn<sup>1</sup>, S. Kempf<sup>1</sup>, S. Lausberg<sup>1</sup>,  
 A. Pabinger<sup>1</sup>, C. Pies<sup>1</sup>, J.-P. Porst<sup>1</sup>, H. Rotzinger<sup>1</sup>, S. Schäfer<sup>1</sup>,  
 R. Weldle<sup>1</sup>, A. Fleischmann<sup>1</sup>, C. Enss<sup>1</sup>, G.M. Seidel<sup>2</sup>

(1) Kirchhoff-Institut für Physik, Universität Heidelberg, INF227, 69120 Heidelberg, Germany  
 (2) Department of Physics, Brown University, Box 1843, Providence, RI 02912, USA

Corresponding author: [loredana.fleischmann@kip.uni-heidelberg.de](mailto:loredana.fleischmann@kip.uni-heidelberg.de)

**Abstract** - An increasing number of experiments employ low temperature radiation/particle detectors which are based on a calorimetric detection scheme and operate at temperatures below 100mK. Metallic magnetic calorimeters use a metallic paramagnetic temperature sensor in tight thermal contact with the x-ray absorber. The magnetization of the sensor is used to monitor the temperature change of the detector upon the absorption of single photons, which is proportional to the absorbed energy. Low-noise high-bandwidth dc-SQUIDs read out the small changes in magnetization. An energy resolution of  $\Delta E_{FWHM} = 2.7\text{eV}$  was obtained for x-ray energies up to 6 keV.

Submitted July 30, 2008. Accepted after revision November 4, 2008. Reference No. CR11; Category 4.

### I. INTRODUCTION

During the last twenty years, the development of low temperature micro-calorimeters progressed rapidly to meet the increasing demand for highly sensitive energy dispersive detectors. The detection principle of these calorimetric detectors is based on the fact, that the absorption of a particle of energy  $E$  in a detector characterized by a heat capacity  $C$  results in an increase of temperature  $\Delta T = E/C$ . Low temperature micro-calorimeters work at temperatures below 100 mK so that the heat capacity contributions due to phonons,  $C_{ph} \propto T^3$ , and electrons,  $C_{el} \propto T$ , are reduced. The detectors are composed of a particle absorber, designed to have a high stopping power for the particles to be detected, strongly coupled to a temperature sensor which has a weak thermal link to a thermal bath. Different solutions are applied for transducing the temperature change resulting from the detected signal into a voltage pulse. The state of the art of temperature transducers for low temperature microcalorimeters is summarized in [1].

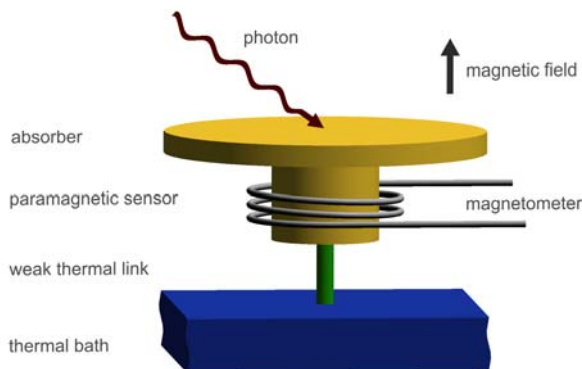


**Fig. 1** Principle drawing of an MMC. The paramagnetic sensor is placed in a weak external magnetic field. The absorption of a particle increases the temperature and thus decreases the magnetization of the sensor. This change is read out by a low-noise high-bandwidth SQUID magnetometer.

Metallic magnetic calorimeters (MMC) use as temperature sensor a paramagnetic material located in a weak magnetic field. The change of the detector temperature  $\Delta T$  upon the absorption of energy leads to a change of the sensor magnetization  $M$  which generates a change of magnetic flux  $\Delta\Phi$  in a pickup coil. This process can be summarized by

$$\Delta\Phi \propto \frac{\partial M}{\partial T} \Delta T = \frac{\partial M}{\partial T} \frac{E}{C} = \frac{\partial M}{\partial T} \frac{E}{C_a + C_s}, \quad (1)$$

where the total heat capacity  $C$  of the detector is the sum of the heat capacity  $C_a$  of the absorber and that of the sensor,  $C_s$ . A sketch of an MMC is shown in Figure 1. The paramagnetic sensor is placed in a small external magnetic field and has a weak thermal link to the thermal bath. The absorption of a particle increases the temperature and thus decreases the magnetization of the sensor. This is read out by a low noise, high bandwidth SQUID magnetometer. With a previously discussed detector prototype for high resolution x-ray spectroscopy an instrumental linewidth of  $\Delta E_{\text{FWHM}} = 3.4$  eV for energies up to 6 keV had been achieved [18]. This resolving power is still poorer than that of wavelength dispersive detectors, but it is very well suited for separation of even closest lines in x-ray fluorescence analysis. It is even sufficient to identify the chemical bonding state of the numerous elements by the chemical shift of characteristic lines.

## II. THEORETICAL AND EXPERIMENTAL BACKGROUND

There are two main reasons for monitoring the temperature *via* magnetic properties of solids: (1) these properties are strongly dependent on temperature and (2) there exist highly sensitive methods to read-out magnetization changes. In the following, the properties of the sensor material and the detector read-out will be discussed.

### A. Sensor material

The first approach to using paramagnetic material as temperature sensor for low temperature detectors was presented by Umlauf *et al.* [2]. In these early prototypes a dielectric material doped with  $^{168}\text{Er}$  ions was used to read out the temperature change upon the interaction of alpha particles in a silicon energy absorber. However, the time response of dielectric paramagnetic materials is determined by the spin-phonon relaxation time which can be of the order of seconds at millikelvin temperatures.

The problem of long relaxation time can be overcome by embedding the magnetic ions in metallic or semi-metallic host-materials [3], where the strong coupling between conduction electrons and localized spins leads to rapid thermalization, well below a microsecond. The presence of the conduction electrons results also in an enhanced interaction between the localized magnetic moments via the Ruderman-Kittel-Kasuja-Yoshida (RKKY) interaction. This indirect exchange interaction represents a drawback since it reduces the temperature dependence of the magnetization and, together with the conduction electrons, increases the heat capacity of the sensor. Therefore materials with very small RKKY interaction are preferred. Paramagnetic alloys based on noble metal hosts that are doped with several hundred ppm of rare earth ions offer a reasonable compromise between the response time and signal size. In addition, these materials are chemically stable and can be machined by standard and microfabrication techniques. The sensor material, which has been studied mostly thus far, is gold doped with erbium (Au:Er)<sup>1</sup>.

---

<sup>1</sup> The matrix element (Au) is underlined to remove ambiguity.

### B. Properties of $\text{Au:Er}$

At low concentrations, erbium forms a solid solution with gold [4].  $\text{Er}^{3+}$  ions substitute  $\text{Au}^+$  ions at regular lattice sites of the fcc matrix. The paramagnetic behaviour of  $\text{Au:Er}$  is caused by electrons of the  $4f$  shell of Er, which is only partially filled and located deep inside the Er ion. Therefore, the interaction with conduction electrons and with the crystal field is reduced and the magnetic moment can be calculated from the orbital angular momentum  $L$ , the spin  $S$  and the total angular momentum  $J$  which are derived according to the Hund's rules. At temperatures above 100 K the magnetization of dilute  $\text{Au:Er}$  alloys is described well by the magnetic moment  $\mu = g_J J$  of the erbium ions, where  $g_J = 6/5$  is the Landé factor and  $J = 15/2$ . At lower temperature it is necessary to include the crystal field in the description [5]. This induces the splitting of the sixteen-fold degeneracy of the  $\text{Er}^{3+}$  ground state into a series of multiplets, out of which the  $\Gamma_7$ -Kramers doublet has lowest energy. It is separated by  $\Delta E = k_B \times 17$  K from the higher multiplets;  $k_B$  is the Boltzmann constant [6]. As a consequence, at temperatures well below 1 K and in small magnetic fields, the magnetization of dilute  $\text{Au:Er}$  alloys can be described well by treating it as a two level system with an effective spin of  $S = 1/2$  and an isotropic  $g$ -factor of  $g = 6.8$  [7]. The performance of MMCs strongly depends on the heat capacity and the magnetization of the  $\text{Au:Er}$  sensors, both of which being dominated by the contribution of the Er ions. Since the working temperature of these detectors is in the range between 10 mK and 100 mK, the Er ions occupy only the states of the  $\Gamma_7$  doublet. To calculate the expected signal of an MMC, both the magnetic dipole-dipole interaction and the indirect exchange interaction between the spins must be taken into account, which can be done accurately by numerical calculations, as discussed in [8]. As an example, Figure 2 compares the measured temperature dependencies of specific heat and magnetization of a  $\text{Au:Er}_{300\text{ppm}}$  sample with results of numerical calculations – at several values of applied magnetic field. The very good agreement allows us to use calculations to predict and optimize the performance of MMCs for a given application by numerical means.

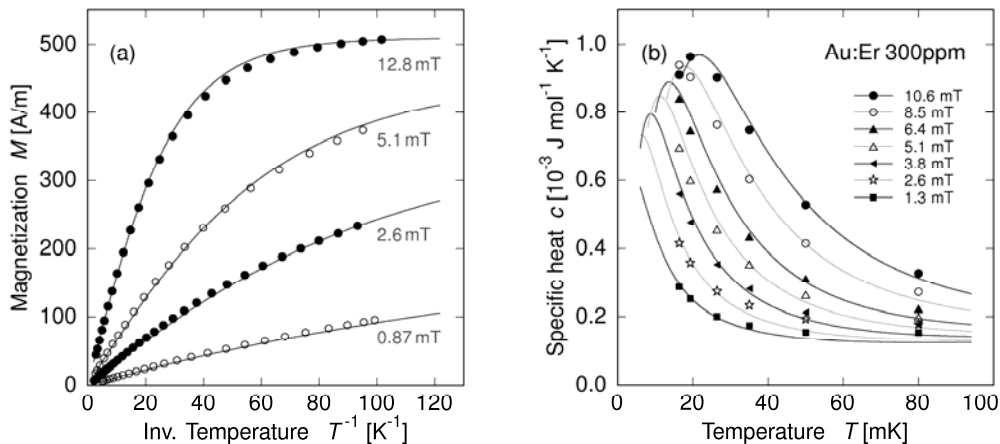


**Figure 2** Magnetization and specific heat of  $\text{Au:Er}$  with a concentration of 300 ppm of isotopically enriched  $^{166}\text{Er}$ . The measured values are indicated by dots and other graphic symbols, the results of numerical calculations are indicated by continuous lines.

### C. SQUID-based Detector Readout

To fulfill the requirements of different applications, the sensor and the pickup coil of a MMC can be designed in various geometries. To date, studies concentrated on two classes of shapes: cylindrical sensors with circular or solenoidal pickup coils [8, 9], and planar sensors with meander-shaped pickup coils [8, 10, 11]. The change of magnetization of the sensor can be detected by a pick-up coil and transferred to the SQUID by a superconducting flux transformer, or the sensor can be placed directly in

the SQUID loop itself. The latter readout scheme has the advantage of not suffering of signal loss due to transformer coupling. However, the sensor temperature is affected by the power dissipation on the SQUID chip. To limit this effect and to decrease the readout electronic noise, the signal from the detector SQUID is amplified by a second (amplifier) SQUID. Figure 3 shows schematically the readout chain for a cylindrical paramagnetic sensor that is positioned directly in the SQUID loop. The two SQUIDs are biased by currents  $I_{b1}$  and  $I_{b2}$ . Any change of flux in the detector SQUID,  $\Phi_1$ , causes a change of current  $\delta I_1$  flowing through the input coil of the amplifier SQUID. This leads to a change of magnetic flux in the secondary SQUID of  $\delta \Phi_2 = M_i \delta I_1$ , where  $M_i$  is the mutual inductance between the input coil of the amplifier SQUID and the SQUID itself. This leads to a small-signal flux-to-flux amplification of:

$$G_\Phi = \frac{\partial \Phi_2}{\partial \Phi_1} = M_i \left( \frac{\partial I_1}{\partial \Phi_1} \right)_{R_g, I_b} = M_i / M_{dyn} \quad (2)$$

at the working point defined by the used load resistance  $R_g$  and the value of  $I_b$ . The term in brackets is the intrinsic current sensitivity of the detector SQUID,  $M_{dyn}$ . In the flux-locked-loop (FLL) mode of operation, the voltage across the secondary SQUID is the input of the feedback, coupled to the detector SQUID *via* the mutual inductance  $M_{fb}$  which provides compensation flux in the detector SQUID. Due to the flux-to-flux gain  $G_\Phi$  and to the transfer coefficient  $\partial V_2 / \partial \Phi_2$  of the amplifier SQUID, the contribution of the input noise of the room temperature electronics to the apparent flux noise of the detector SQUID can be strongly reduced. At the same time, the power dissipation in the detector SQUID can be kept reasonably small, as it can be operated at low voltage values using a small  $R_g$ .

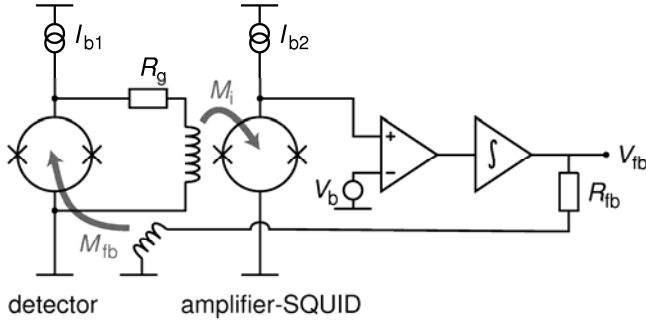


**Figure 3:** Simplified circuit schematics of a two-stage SQUID readout with FLL electronics, as used with MMCs.

The working temperature of the detector SQUID is usually below 100 mK while the amplifier SQUID can be operated at the same temperature or between 1 K and 4.2 K, depending on the particular case.

#### D. Noise Sources

The energy resolution of magnetic calorimeters is determined mainly by four sources of noise: the thermal fluctuations of energy between the subsystems of the detector and the thermal bath, the magnetic Johnson noise caused by the thermal motion of electrons in the metallic parts of the detector, the flux noise of the SQUID magnetometer and the still not completely understood  $1/f$  noise contribution, which seems to be caused by the magnetic moments of the sensor and to be independent of the temperature [12]. Of these four contributions, only the thermodynamic fluctuations of energy are directly related to the calorimetric detection scheme, being independent of the readout techniques. It has been shown in [13] that these energy fluctuations lead to a fundamental limit of the energy resolution of the MMC which can be written as:

$$\Delta E_{FWHM} = 2.35 \sqrt{4k_B C_a T^2} \left( \frac{1}{\beta(1-\beta)} \frac{\tau_0}{\tau_1} \right)^{1/4}. \quad (3)$$

Here,  $\tau_0$  is the rise time of the detector signal,  $\tau_1$  is the decay time of the detector signal and  $\beta = C_s/C_{\text{tot}}$  is the fraction of heat capacity that is due to the spin system.

At present, the limit where the energy resolution is dominated by the thermal fluctuations of energy is not yet achieved and the energy resolution still suffers from a significant contribution of other noise sources. The magnetic Johnson noise depends on the sensor and pickup coil geometry and obeys the proportionality

$$S_\phi \propto \sigma k_B T, \quad (4)$$

where  $\sigma$  is the electric conductivity of the sensor and absorber. The white magnetic flux noise in the detector SQUID can be expressed by

$$S_\phi = S_{\phi,1} + \frac{4k_B TR_g}{(\partial V_1 / \partial \Phi_1)_{R_g}^2} + \frac{S_{\phi,2}}{G_\phi^2} + \frac{S_{V,\text{el}}}{(\partial V_1 / \partial \Phi_1)^2 G_\phi^2}. \quad (5)$$

Here,  $S_{\phi,1}$  and  $S_{\phi,2}$  represent the intrinsic SQUID noise of the detector and amplifier SQUIDs,  $\partial V_1 / \partial \Phi_1$  is the slope of the detector SQUID characteristic, and  $\partial V_2 / \partial \Phi_2$  is that of the amplifier SQUID.

These two noise contributions mentioned above can in principle be reduced by controlling the electric conductivity to limit the magnetic Johnson noise, and by using very low noise SQUIDs. To put the importance of these contributions into perspective, we discuss the expected linewidth of a fully optimized MMC for high resolution x-ray spectroscopy with  $C_a = C_s = 0.2$  pJ/K,  $\tau_0 = 1$   $\mu$ s and  $\tau_1 = 1$  ms that is operated at a temperature of 50 mK. From the equation (3) we derive a fundamental limit for the energy resolution of this detector of  $\Delta E_{\text{FWHM}} = 0.62$  eV. This result is hardly modified when the magnetic Johnson noise is included in the calculation, as the electrical conductance  $\sigma$  of the involved materials is typically small enough. Assuming the white flux noise of the detector SQUID to be described by energy sensitivity of  $\varepsilon = 15 h$  and a  $1/f$  flux noise of  $3 \mu\Phi_0/\sqrt{\text{Hz}}$  at 1 Hz, the energy resolution of the detector will be degraded by about 20 % resulting in  $\Delta E_{\text{FWHM}} = 0.75$  eV. Adding the  $1/f$  flux noise, which has been observed in detectors based on Au:Er sensors and attributed to the Er ions, to the noise of the detector discussed here leads to a further degradation by 25 %, resulting in a total linewidth of  $\Delta E_{\text{FWHM}} = 0.95$  eV.

### III. HIGH ENERGY RESOLUTION DETECTOR FOR X-RAY SPECTROSCOPY

#### A. Detector setup

The detector for high resolution x-ray spectroscopy discussed here is based on commercially available SQUID chips. The detector SQUID is a KSUP-10-50 fabricated by IBM [14]. This is a first order gradiometer having two planar loops of 50  $\mu$ m diameter wound in opposite sense. The cylindrical Au:Er sensor, shown yellow in Figure 4(a), is fixed inside one of two gradiometric loops by the epoxy Stycast 1266. The sensor has a diameter of about 50  $\mu$ m, height of 8  $\mu$ m and concentration of 600 ppm of isotopically enriched  $^{166}\text{Er}$ . The square absorber (transparent yellow) is made of high purity gold foil, has a collecting area of 180  $\mu$ m  $\times$  180  $\mu$ m and a thickness of 5  $\mu$ m, resulting in a stopping power of 98% for 6 keV x-ray quanta. It is ultrasound-welded to the Au:Er sensor. This metal-metal contact between absorber and sensor provides a fast thermalization between absorber and temperature sensor, resulting in a fast signal rise. In Figure 4(b) a cross section of the detector setup is shown. The detector is positioned on the SQUID chip, electrical contacts to the SQUID are provided by Al:Si bonding wires. The magnetic field needed to polarize the erbium spins is generated by a wire-wound coil with persistent-current switch, which allows for magnetic fields up to 3 mT in the volume of the Au:Er sensor.

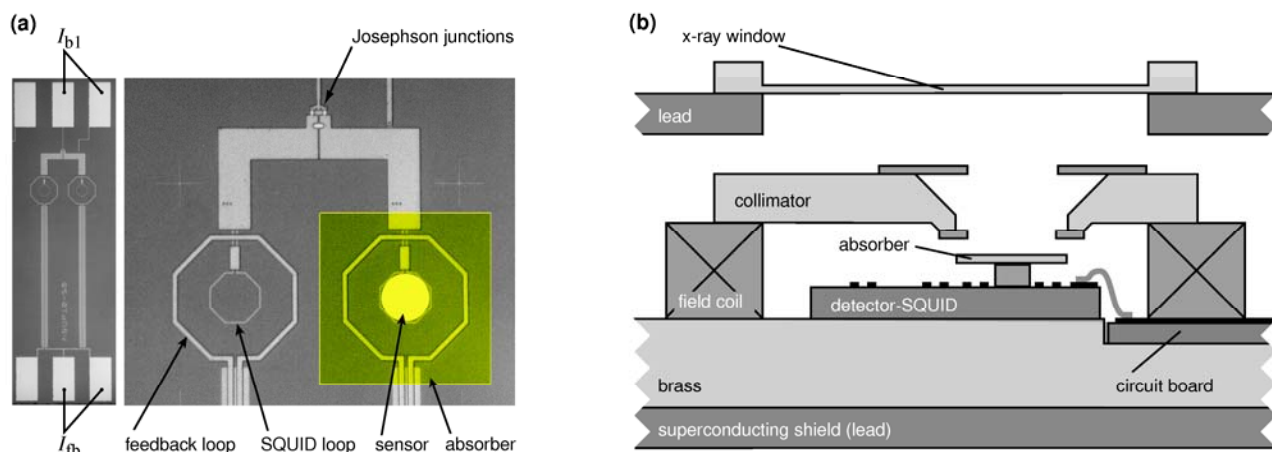


**Figure 4.** (a) Micro-graph of the KSUP-10-50 SQUID with superimposed sketch of the cylindrical Au:Er-sensor and the square Au absorber. (b) Cross section of the detector setup.

The Josephson junctions of the SQUID were covered by a small piece of bulk lead foil in order to shield them from the external field. A collimator prevents x-rays emitted by the external  $^{55}\text{Fe}$  source from hitting the substrate. A 200 nm thick aluminium x-ray window protects the detector from infrared radiation. To shield the detector from fluctuating external magnetic fields a superconducting lead shield is surrounding the entire detector including the brass-holder. The detector was operated at temperatures between 20 mK and 100 mK. These temperatures were provided by a two-stage adiabatic demagnetization refrigerator [15], where the paramagnetic salt pills are precooled by pumped liquid helium at a temperature of 1.8 K. The signal of the detector is passed to the amplifier SQUID of type CCBlue [16] through superconducting NbTi wires in CuNi matrix. The amplifier SQUID is operated at 1.8 K.

### B. Results and Discussion

The energy resolution of the detector was characterized by measuring the x-ray fluorescence spectrum of manganese emitted by an external  $^{55}\text{Fe}$ -source. The detector was operated in a magnetic field of 3 mT at a bath temperature of  $23 \text{ mK} \pm 15 \mu\text{K}$ . Under these conditions, the temperature of the calorimeter mounted on the detector SQUID chip was about 35 mK due to the power dissipated in the SQUID. The absorption of photons of the  $K_{\alpha}$  line with an energy of 5.9 keV caused the temperature of the detector to rise by about 0.75 mK, corresponding to a total heat capacity of 1.25 pJ/K. The fast intrinsic rise time of the magnetization signal, which is well below 1  $\mu\text{s}$ , was not observable in this experiment, as the relatively large inductance of the wires connecting the two SQUIDs resulted in a low-pass characteristic with cut-off frequency of about 500 kHz. The decay time of the transient signals, *i.e.*, the time constant describing the thermalization of the detector with the bath, was 8.1 ms, which is in agreement with the expected Kapitza resistance between the Au:Er sensor and the silicon substrate. Within a measurement time of 3 h a total of 16000 pulses were recorded at an average rate of  $1.5 \text{ s}^{-1}$  as well as 8000 noise traces in between those pulses. An algorithm based on the idea of optimal/matched filtering was used to assign an energy to each digitized trace, consisting of 16384 samples of 12-bit resolution, one quarter of which being prior to the trigger.

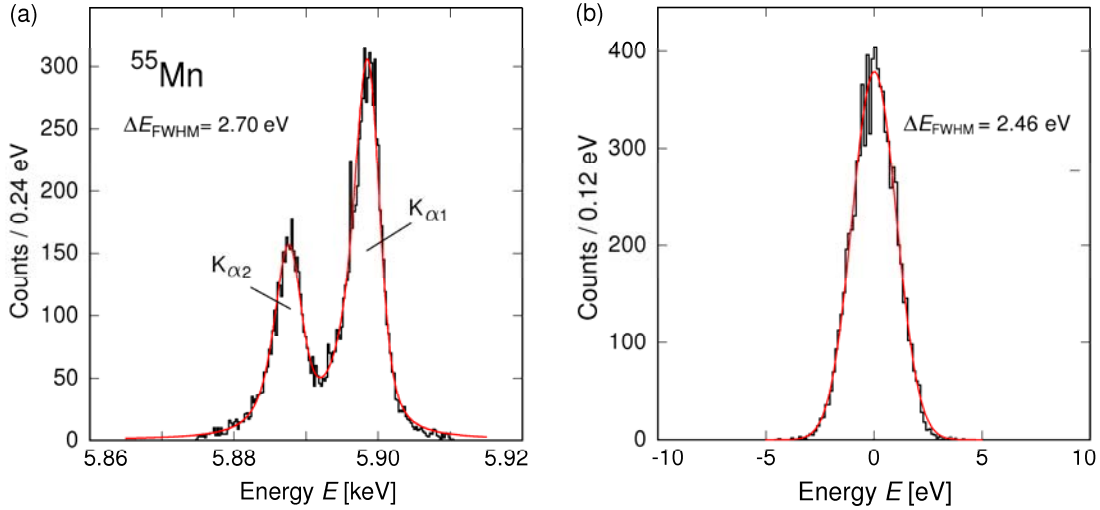


**Figure 5.** (a) Energy spectrum of the Ka line of manganese acquired with the MMC discussed in the text. (b) Energy spectrum obtained by applying the optimal filtering algorithm to untriggered noise traces.

As the temperature stability of the cryostat was not adequate for taking a high-resolution spectrum, and as the detector itself is the most sensitive thermometer in the discussed setup, we used the correlation between pre-trigger signal offset and pulse height to correct for the actual operating temperature and corresponding total signal gain during each event. Figure 5(a) shows the obtained energy histogram of the two  $K_{\alpha}$  lines of manganese at 5.9 keV which are separated by a fine-structure splitting of about 12 eV. The superimposed smooth curve represents the natural line shape as measured by Hölzer et al. [17] convoluted with a Gaussian distribution with  $\Delta E_{\text{FWHM}} = 2.7$  eV. As expected for MMCs, this instrumental line width obtained at 5.9 keV is almost independent of energy, as can be seen from the energy histogram in Figure 5(b), which was generated by applying the optimal filtering algorithm to the untriggered baseline traces and represents the instrumental line shape at zero energy having a width of  $\Delta E_{\text{FWHM}} = 2.5$  eV. The small energy-dependent contribution is likely to be due to limitations of the temperature correction described above. A detailed analysis of the detector signal noise allowed us to identify several contributions to the instrumental linewidth of 2.5 eV. Assuming a noise-free readout, the thermodynamic fluctuations of energy between the subsystems of the detector and the thermal bath would result in an energy resolution of about  $\Delta E_{\text{FWHM}} = 0.4$  eV. Taking the flux noise of the two-stage SQUID setup into account, which can be described by a white noise level of  $1.0 \mu\Phi_0/\sqrt{\text{Hz}}$  and a  $1/f$  noise density of about  $3 \mu\Phi_0/\sqrt{\text{Hz}}$  at 1 Hz, the linewidth is degraded to  $\Delta E_{\text{FWHM}} = 1.15$  eV. A further contribution to the  $1/f$  noise with a noise density of about  $30 \mu\Phi_0/\sqrt{\text{Hz}}$  at 1 Hz seems to be caused by the Er-ions of the sensor material itself; it resulted in a total linewidth of  $\Delta E_{\text{FWHM}} = 1.6$  eV. This is about the energy resolution that we expected to obtain while designing and fabricating the detector; it takes into account all noise contributions known to be inherently present in the detector signal. An additional and not foreseen noise contribution degraded the intrinsic linewidth of the detector to be 2.5 eV and therefore about 1.6 times larger than the design value. The power density of this noise contribution increases towards low temperatures and its spectral shape resembles that of the thermodynamic energy fluctuations between the sensor and the thermal bath provided by the silicon substrate. Both properties suggest that this contribution is caused by fluctuating chip temperature, which in turn might be caused by fluctuations of the power dissipated in the SQUID. This interpretation is supported by the fact, that this noise contribution is not observed, if both gradiometric SQUID loops are equipped with paramagnetic sensors [18].

To put the present state of magnetic calorimeters for high resolution x-ray spectroscopy in some perspective, we want to compare their properties briefly to those of transition edge sensors (TES) [19]. The latter are calorimetric detectors as well, but make use of the steep  $R(T)$  characteristics of a superconducting thin film biased at the transition between normal conducting and superconducting state to measure the change of temperature upon the deposition of energy. Presently, the energy resolution achieved by TES-calorimeters is 1.8 eV at 5.9 keV [20]. Despite the obvious differences of these two types of temperature sensors, it seems plausible at present that both techniques will get very close to energy resolutions that are dominated by the thermo-dynamical fluctuations of energy, only depending on the heat capacity of the detector, the temperature and the thermal relaxation times of the detector response.

However, looking at details of design, fabrication and operation, the two types of detectors appear to be quite different. TES sensors have been developed and optimized in detail by numerous groups for more than two decades. In order to secure a transition temperature below 100 mK, different proximity effect bi-layers and superconducting alloys have been studied to find candidates that don't suffer from aging. Excess noise, observed in early TES designs, was greatly reduced by optimizing the structure of the normal metal and superconducting layers. Among others, there might be three properties of TES sensors, that make them a very attractive candidate for applications, where detector arrays with high count rate capabilities are required: (i) The intrinsic negative electro-thermal feedback, that can reduce the thermal recovery time of the detector significantly, (ii) the large primary signal, which relaxes the requirements for amplifier noise, (iii) the resistance of the TES sensor can be small enough to form, together with the input coil inductance of the readout SQUID, a sufficiently low-pass anti-aliasing filter that is necessary for time-domain multiplexing without noise degradation. However, making use of these benefits requires a good knowledge of the electro-thermal properties of the fabricated structures, detailed modelling and excellent clean room facilities.

The probably most fundamental difference between magnetic calorimeters and TES-based calorimeters is the fact, that the measurement of the magnetization of a paramagnetic sensor by a SQUID is essentially dissipationless. In addition, presently developed magnetic calorimeters make use of the almost Curie-like paramagnetism of chemically and physically stable dilute noble metal alloys, a property that is well described by thermodynamical means and expected to be stable and not affected by aging. However, due to the comparably weak temperature dependence of the Curie-law, the primary signal of the sensor is small compared to that of TES sensors and some care has to be taken to keep the noise of the readout circuit small. For most applications the low noise readout can be guaranteed, opening up the possibility to benefit from a number of advantages of MMCs. (i) Both MMCs made from bulk material, as discussed here, as well as those micro-fabricated are described by standard statistical physics and the signal as well as the noise can be modeled with confidence allowing for a numerical optimization of detector designs for particular applications. (ii) An MMC, optimized for the operation at a particular working temperature, can also be operated at different temperatures, but with a somewhat degraded energy resolution. However, there is no threshold temperature like the  $T_c$  of TES sensors above (and below) which the operation of the detector becomes impossible. This property relaxes some constraints in the thermal design of large detector arrays. (iii) Assuming superconducting flux transformer coupling between sensor and SQUID, the power dissipation in the vicinity of the sensor can be kept arbitrarily small. Together with the fact (iv) that the sensors have no electrical connection to the readout circuit, this add additional flexibility in the electro-thermal design of large arrays. (v) As sensor and absorber are based on normal metals and as the Korringa-time describing the electron-spin relaxation time is below 1  $\mu$ s even at milli-Kelvin temperatures, MMCs can be designed with very fast signal rise times. To date, the fastest reported rise time is as short a 70 ns [21]. The short rise time in combination with the dissipationless nature of the initial signal meets a set of requirements for a multiplexed readout circuitry, which is quite different from the one used for TES sensors.

Furthermore, it is a great benefit for applications where timing information or pile-up suppression is needed.

At present two approaches seem to be promising: First, time domain multiplexing after the first-stage SQUIDs of a detector array [22]. Second, frequency domain multiplexing of rf-SQUIDs, which are coupled to coplanar  $\lambda/4$  microwave resonators arranged along a transmission line and read out by a cold HEMT amplifier. The latter concept seems especially attractive for very large arrays, because a large number of channels can be summed in one cable and brought to room temperature. In addition the power dissipation at low temperatures is reduced to a minimum [23].

## V. CONCLUSION AND OUTLOOK

New generations of high-energy resolution magnetic calorimeters have been developed and soon they will be field-tested. Two different approaches shall be followed. The natural successor of the discussed detector follows the same concept but uses a gradiometer SQUID with a loop diameter of  $20\mu\text{m}$ . This is nowadays possible with the help of microfabrication techniques and due to the reliability achieved in the sputtering of the Au:Er dilute alloys [10]. The second approach is the use of planar Au:Er sensors with transformer-coupled meander shaped pick-up coils [11,10]. In this configuration, the change of magnetization of the sensor is read out by a meander pickup coil, which at the same time provides the magnetic field to polarize the sensor material by means of a persistent current frozen in the superconducting loop containing the meander. This second configuration has the advantage of no power dissipation on the detector chip and more flexibility in terms of detecting area. For both of this configurations the expected energy resolution should be below  $\Delta E_{\text{FWHM}} = 1 \text{ eV}$ .

## ACKNOWLEDGMENT

This work was supported by the DFG (Grant En299/3) and the BMBF (Grant F&E 13N8226).

## REFERENCES

- [1] C. Enss (ed.), "Cryogenic Particle Detection", *Topic of Applied Physics* **99**, Springer-Verlag Berlin Heidelberg (2005).
- [2] E. Umlauf and M. Bühler, "A magnetic Bolometer for single particle detection", *Europhys. Lett.* **5(4)**, 297-301 (1988).
- [3] S. Bandler, C. Enss, R.E. Lanou, H.J. Maris, T. More, F.S. Porter and G.M. Seidel, "Metallic Magnetic Calorimeter for Particle Detection", *J. Low Temp. Phys.* **93(3)**, 709-714 (1993).
- [4] P.E. Rider and K.A. Geschneider Jr. and O.D. McMaster, "Gold-rich rare-earth-gold solid solution", *Transaction of the Metallurgical Society of Aime* **233**, 1488-1496 (1965).
- [5] G. Williams und L.L. Hirst, "Crystal-Field Effects in Solid Solutions of Rare Earths in Noble Metals", *Phys. Rev.*, **185(2)**, 407-414 (1969).
- [6] W. Hahn, M. Löwenhaupt and B. Frick, "Crystal field excitation in dilute rare earths noble metal alloys", *Physica B* **180-181**, 176-178 (1992).
- [7] L.J. Tao, D. Davidov, R. Orbach and E.P. Chock, "Hyperfine Splitting of Er and Yb Resonance in Au: A Separation between the Atomic and Covalent Contributions to the Exchange Integral", *Phys. Rev. B* **4(1)**, 5-9 (1971).
- [8] A. Fleischmann, C. Enss, G.M. Seidel, "Metallic Magnetic Calorimeters", *Topic of Applied Physics* **99**, 151-216 (2005).
- [9] M. Loidl, E. Leblanc, M. Rodrigues, J. Bouchard, B. Censier, T. Branger and D. Lacour, "[Metallic Magnetic Calorimeters for Absolute Activity Measurement](#)", *Journal of Low Temp. Physics* **151 (3/4)**, 1055-1060 (2008).
- [10] A. Burck, S. Kempf, S. Schäfer, H. Rotzinger, M. Rodrigues, T. Wolf, L. Gastaldo, A. Fleischmann, C. Enss, "Micro-

- structured magnetic calorimeter with meander-shaped pickup coil", *J. of Low Temp. Physics* **151** (1/2), 337-344 (2008).
- [11] B.L. Zink, K.D. Irwin, G.C. Hilton, D.P. Pappas, J.N. Ullom and M.E. Huber, "Lithographically patterned magnetic calorimeter X-ray detectors with integrated SQUID readout", *Nucl. Inst. Meth A* **520** (1-3), 52-55 (2004).
- [12] T. Daniyarov, "[Metallische magnetische Kalorimeter zum hochauflösenden Nachweis von Röntgenquanten und hochenergetischen Molekülen](#)", Dissertation, Universität Heidelberg, Germany (2005).
- [13] A. Fleischmann, "High Resolution X-Ray Detection Using Metallic Magnetic Calorimeters", *Adv. Solid State Phys.* **41**, 577-587 (2001).
- [14] M.B. Ketchen, D.D. Awschalom, W.J. Gallanger, A.W. Kleinsasser, R.L. Sandstrom, J.B. Rosen and B. Bumble, "Design, fabrication, and performance of integrated miniature SQUID", *IEEE Trans. Mag.* **25**, 1212-1215 (1989)
- [15] Vericoltd Technologies GmbH, Ismaning, Germany.
- [16] Supracon AG, Jena, Germany.
- [17] G. Hölzer, M. Frisch, M. Deutsch, J. Hartwig and E. Förster, " $K_{1,2}$  and  $K_{1,2}$  x-ray emission lines of the 3d transition metals", *Phys. Rev. A* **56**, 4554-4568 (1997).
- [18] A. Fleischmann, M. Linck, T. Daniyarov, H. Rotzinger, C. Enss and G.M. Seidel, "Metallic magnetic calorimeters (MMC): detectors for high-resolution X-ray spectroscopy", *Nucl. Inst. Meth B* **520** (1-3), 27-31 (2004).
- [19] K. D. Irwin and G. C. Hilton, "Transition-Edge Sensors", *Topic of Applied Physics* **99**, 63-150 (2005).
- [20] S. R. Bandler, R. P. Brekosky, A. D. Brown, J. A. Chevernak, E. Figueroa-Feliciano, F. M. Finkbeiner, N. Iyomoto, R. L. Kelley, C. A. Kilbourne, F. S. Porter, J. Sadleir, S. J. Smith "Performance of TES X-ray Microcalorimeters with a Novel Absorber Design", *J. of Low Temp. Physics* **151** (1/2), 400-405 (2008).
- [21] H. Rotzinger, J. Adams, S. R. Bandler, J. Beyer, H. Eguchi, E. Figueroa-Feliciano, W. Hsieh, G. M. Seidel, T. Stevenson "Performance of Micro-fabricated Magnetic Calorimeters Arrays for X-ray Spectroscopy", *J. of Low Temp. Physics* **151** (1/2), 351-356 (2008).
- [22] J. Beyer, D. Drung, "A novel single-stage SQUID multiplexer for TES array readout", *Supercond. Sci. Technol.* **21**, 105022 (2008).
- [23] J. A. B. Mates, G. C. Hilton, K. D. Irwin, L. R. Vale, K. W. Lehnert "Demonstration of a Multiplexer of Dissipationless SQUIDS", *Appl. Phys. Lett.* **92**, 023514 (2008).